



ELSEVIER

Available online at [www.sciencedirect.com](http://www.sciencedirect.com)

SCIENCE @ DIRECT®

Surface and Coatings Technology 177–178 (2004) 65–72

**SURFACE  
& COATINGS  
TECHNOLOGY**

[www.elsevier.com/locate/surfcoat](http://www.elsevier.com/locate/surfcoat)

## LaCrO<sub>3</sub>-based coatings on ferritic stainless steel for solid oxide fuel cell interconnect applications

J.H. Zhu<sup>a,\*</sup>, Y. Zhang<sup>a</sup>, A. Basu<sup>a</sup>, Z.G. Lu<sup>a</sup>, M. Paranthaman<sup>b</sup>, D.F. Lee<sup>c</sup>, E.A. Payzant<sup>c</sup>

<sup>a</sup>Department of Mechanical Engineering, Box 5014, Tennessee Technological University, Cookeville, TN 38505, USA

<sup>b</sup>Chemical Sciences Division, Oak Ridge National Laboratory, Oak Ridge, TN 37831, USA

<sup>c</sup>Metals and Ceramics Division, Oak Ridge National Laboratory, Oak Ridge, TN 37831, USA

### Abstract

A thin layer of doped lanthanum chromite on ferritic steel may act as a protective coating to mitigate the Cr volatility problems and facilitate the use of metallic interconnect in solid oxide fuel cells operated at intermediate temperatures. In this paper, the LaCrO<sub>3</sub> thin film was successfully synthesized on a ferritic stainless steel substrate by two approaches, i.e. reactive formation and sol–gel processing. The coating structures and surface morphologies were analyzed using X-ray diffraction and scanning electron microscopy. After isothermal oxidation at 850 °C for 100 h in air, the electrical resistance of the sol–gel coated samples remained very low, as compared to that of the uncoated sample after similar thermal exposure. The sol–gel coating also provided effective protection for the interconnect steel during oxidation of twelve 100-h cycles at 800 °C in air, whereas significant spallation and weight loss were observed for the uncoated steel. The two coating processes (i.e. reactive formation and sol–gel processing) were compared and their advantages and drawbacks were outlined.

© 2003 Elsevier B.V. All rights reserved.

**Keywords:** Ferritic stainless steel; Sol–gel processing; Solid oxide fuel cell

### 1. Introduction

In the planar design of a solid oxide fuel cell (SOFC) stack, the interconnect acts not only as electrical connection between the single cells but also as the mechanical support of the thin electroactive ceramic parts and as gas-proof separation of fuel gas (e.g. hydrogen or methane) and oxidant (e.g. air). Furthermore, the interconnects distribute the gas in co-, cross- and/or counter-flow and act as constructional connection to the external gas inlets and outlets. Because of the high operating temperatures (up to 1000 °C), the requirements for interconnect materials are quite stringent, and a satisfactory solution has not been found so far. An interconnect material must fulfill the criteria listed below:

- High density (no open porosity). The material must be impervious to gases to avoid mixing of air and fuel.
- High electronic and negligible ionic conductivity.

- High creep resistance. The material should not creep during fuel cell operation.
- High thermal conductivity ( $>20 \text{ W m}^{-1} \text{ K}^{-1}$  [1]) for uniform heat distribution in the stack.
- Chemical and physical stabilities in both oxidizing and reducing environments and also with respect to cathode and anode.
- Match in coefficient of thermal expansion (CTE) with other cell components at the fuel cell operating temperature and during thermal cycling.

Metallic interconnects are preferred over the conventional ceramic interconnects, for planar-type SOFC, due to their superior electronic and heat conductivity and low-cost [2–6]. With the current trend in reduction of the SOFC operating temperature to less than 800 °C, the demands on interconnect material are less severe. As a consequence, ferritic stainless steels have become the candidate material for interconnect due to their close match of CTE with solid electrolyte, and their initial success as interconnect material has been demonstrated [7–11]. One major concern with ferritic steels is their long-term stability and compatibility issues, which are

\*Corresponding author. Tel.: +1-931-372-3186; fax: +1-931-372-6340.

E-mail address: [jzhu@tntech.edu](mailto:jzhu@tntech.edu) (J.H. Zhu).

related to the Cr volatility and non-protective oxide products [12]. Furthermore, over long-term exposure during SOFC operation, the ferritic steel may react with the  $\text{LaMnO}_3$  cathode to form some reaction layers and thus reduce the performance of a stack. Indeed, it was found that during thermal exposure, duplex layers of Mn–Cr spinel outer layer and  $\text{Cr}_2\text{O}_3$  inner layer were formed upon interaction of the steel with  $\text{LaMnO}_3$  component [10,11]. To solve these potential problems, low-cost surface coatings need to be developed, which should be dense, electronically conductive, non-volatile and chemically compatible with other cell components.

Several surface coatings have been used to improve the oxidation resistance and electronic conductivity of chromia-forming alloys over the past few years [13–21], i.e. pre-oxidation in a controlled environment to form dense, adherent  $\text{Cr}_2\text{O}_3$  scale [13], electron-beam physical vapor deposition of La layer [14,15] and spray painting of La/Sr oxide layer [16] to form a  $\text{LaCrO}_3$ -type coating upon thermal exposure, thermal spray to directly deposit a perovskite coating on the metallic interconnect [17]. All these coatings led to improved scale adherence and scale electronic conductivity, while reducing oxide growth rate and Cr volatility.

In this paper, we investigated the feasibility of depositing a thin, dense, conductive  $\text{LaCrO}_3$ -based coating on ferritic stainless steel using two cost-effective fabrication routes (reactive formation and sol–gel process). The surface morphology and coating structure were characterized. Furthermore, the effects of sol–gel coating on the oxidation behavior of the interconnect alloy and electrical resistance of the oxide scale after thermal exposure in air were investigated. The advantages and drawbacks of the two coating processes were discussed in the light of the experimental results.

## 2. Experimental

### 2.1. Substrate material

A commercial ferritic stainless steel (Type 444) was selected for this study. The chemical composition, as provided by the industrial supplier, was Fe–0.011C–17.75Cr–1.89Mo–0.44Si–0.26Mn–0.2Ti–0.25Nb–0.23Ni (wt.%). The steel sheet was cut into small pieces of  $15 \times 11 \times 1.5 \text{ mm}^3$  by an electric discharge machine and the samples were carefully polished to a  $0.3\text{-}\mu\text{m}$  finish using alumina abrasives. The samples were cleaned ultrasonically in acetone for 5 min and then in methanol for 10 min prior to coating.

### 2.2. Coating processing

Two separate methods were used to deposit  $\text{LaCrO}_3$  (Sr-doped or undoped) coating on the samples. The first method is termed ‘reactive formation’, where three steps

were involved: (1) the steel samples were annealed at 900–1200 °C in a reducing environment ( $\text{Ar} + 4\% \text{H}_2$ ), i.e. in low partial pressure oxygen, which led to the preferential formation of a thin, dense and adherent  $\text{Cr}_2\text{O}_3$  layer; (2) La oxide was then deposited on the sample surface by means of r.f. sputtering for 4–5 h, using a  $\text{La}_2\text{O}_3$  target; (3) the samples were then annealed in air so that the thermally grown  $\text{Cr}_2\text{O}_3$  layer and the sputtered  $\text{La}_2\text{O}_3$  layer could react to form  $\text{LaCrO}_3$  layer. The optimal reaction conditions for forming the  $\text{LaCrO}_3$  layer were determined by varying the reaction temperature (from 800 to 1000 °C) and reaction time (from 10 min to 5 h).

In the second method, the  $(\text{La}_{1-x}\text{Sr}_x)\text{CrO}_3$  thin films with different levels of Sr doping ( $x=0, 0.1, 0.2$  and  $0.3$ ) were obtained by a sol–gel process based on organic chelating precursors. The solution for obtaining the desired  $(\text{La}_{1-x}\text{Sr}_x)\text{CrO}_3$  coating was prepared using appropriate amounts of high-purity La nitrate (Alfa Aesar, REaction<sup>®</sup>, 99.99% pure), Sr nitrate (Alfa Aesar, Puratronic<sup>®</sup>, 99.9965% pure), Cr nitrate (Alfa Aesar, Puratronic<sup>®</sup>, 99.999% pure), citric acid and distilled water. The solutions were mixed together and heated in a hot plate to get precursor solutions with specific concentrations. A magnetic stirrer was used to ensure homogenous mixing. The films were deposited on the substrate by both spin-coating and dip-coating techniques. For spin coating, the sample with certain amount of the solution on it was rotated at an average speed of 2000 rpm for 15 s. For dip coating, the sample was pulled out of the solution at a linear speed of  $0.05 \text{ cm s}^{-1}$ . The coated samples were then dried and annealed at elevated temperature to form the desired phase in the coatings. For high-temperature X-ray diffraction (XRD) study, the coatings were obtained using a 0.5 M solution to get relatively thick coatings. However, such coatings were relatively porous; therefore, a 0.3 M solution was used to coat the steel substrate for oxidation and electrical resistance study. Since the coating thickness was less than  $1 \mu\text{m}$  after one coating run with the 0.3 M solution, the entire procedure was repeated six times (six passes) to increase the coating thickness, with an intermediate anneal of 800 °C for 1 h in air.

### 2.3. Characterization of the coatings

Room-temperature XRD patterns were obtained using a Philips XRD unit. To determine the optimal conditions for forming the  $(\text{La}_{1-x}\text{Sr}_x)\text{CrO}_3$  phase in the sol–gel coatings, a high-temperature XRD (Scintag PAD X) was used to monitor the phase changes as the coated sample was heated in situ in the sample chamber (Buehler HDK 1.4) of the diffractometer. Surface morphologies and cross-sections were observed using a scanning electron microscope (SEM) (Hitachi S-4100).

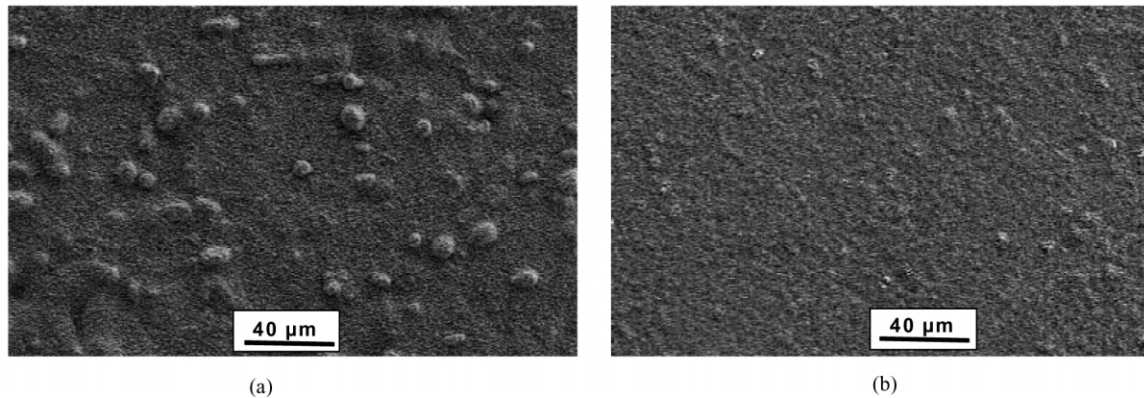


Fig. 1. SEM surface morphologies of SS-444 samples annealed at 1000 °C for 5 h (a) in air and (b) in Ar+4% $H_2$  environment.

The electrical resistance of the sol–gel coated samples before and after isothermal exposure in air (850 °C for 100 h) was measured from 600 to 900 °C using a four-point DC set-up. An uncoated substrate specimen was also oxidized in the same condition and its electrical resistance was measured for comparison. Pt electrodes were made by covering the two surfaces with Pt paste followed by placing Pt meshes on top of the paste as current collectors. A current source was used to provide a constant current of 0.1 A and the resulting voltage drop across the sample was measured using a multimeter.

The effects of coating on the oxidation behavior of the steel were studied by monitoring the weight changes of both the sol–gel coated and uncoated samples upon cyclic oxidation. Each cycle consisted of air exposure at 800 °C for 100 h, followed by furnace cooling; the total number of cycles is 12, with a corresponding cumulative exposure time of 1200 h. The surface morphologies of cyclically oxidized samples were examined in the SEM.

### 3. Results and discussion

#### 3.1. Reactive formation

The first step in reactive formation of the  $LaCrO_3$  layer is to form a thin, adherent and uniform  $Cr_2O_3$  layer. Fig. 1 shows the surface morphologies of two SS-444 samples annealed at 1000 °C for 5 h in air (Fig. 1a) and in flowing Ar+4% $H_2$  environment (with an oxygen partial pressure of  $\sim 10^{-13}$  Pa) (Fig. 1b), respectively. The SEM observation indicated that the  $Cr_2O_3$  layer formed by oxidation in low partial pressure oxygen was more uniform and adherent than that formed in air, in agreement with Linderoth [13]. There were many oxide nodules on the sample surface annealed in air, while the surface of the sample annealed in low partial pressure oxygen was much smoother. Apparently, in a low partial pressure of oxygen,  $Cr_2O_3$  is the main stable oxide and it is relatively dense, while oxidation

in air leads to the formation of other non-protective oxides.

Sputtering with a  $La_2O_3$  target for 4–5 h in an Ar+4 $H_2$  environment led to the formation of an amorphous  $La_2O_3$  layer on the pre-oxidized sample. The substrate sample was not heated during sputtering; it was estimated that the substrate temperature should be less than 150 °C during sputtering. The cross-sectional view of the as-sputtered sample is shown in Fig. 2a, clearly illustrating the double-layer structure after sputtering. The top layer was the sputtered  $La_2O_3$  layer with approximately 1- $\mu m$  thickness, while the inner layer was the  $Cr_2O_3$  layer formed by annealing in flowing Ar+4% $H_2$  environment at 900 °C for 6 h. Both the oxide layers were dense and uniform. Note that some second-phase precipitates in the substrate adjacent to the  $Cr_2O_3$  layer were observed. After post-deposition anneal in air (e.g. 1000 °C for 1 h), a  $LaCrO_3$  layer was formed due to the interdiffusion and reaction of the two layers, as shown in Fig. 2b. The reaction involved in the  $LaCrO_3$  formation is given by



This reaction is thermodynamically feasible, with a Gibbs free energy change ( $\Delta G_{298}^0$ ) of  $-78.6 \text{ kJ mol}^{-1}$  [22,23]. The presence of some Kirkendall voids was observed at the initial interface of the two layers, as a result of the interdiffusion of atoms in the two layers. The microstructure in Fig. 2b implied the possibility of incomplete reaction between the two layers after 1 h at 1000 °C. However, XRD indicated that the main phase in the coating was  $LaCrO_3$  after post-deposition anneal. In order to study the kinetics of the reactive formation of  $LaCrO_3$  and the optimal conditions for forming the  $LaCrO_3$  layer, the sputtered coatings were annealed in air at 800, 900 and 1000 °C for various times. Typical results are shown in Fig. 3, for a sample annealed in air at 800 °C for different times. Fig. 3a shows the XRD pattern of the as-sputtered sample, where the main peaks

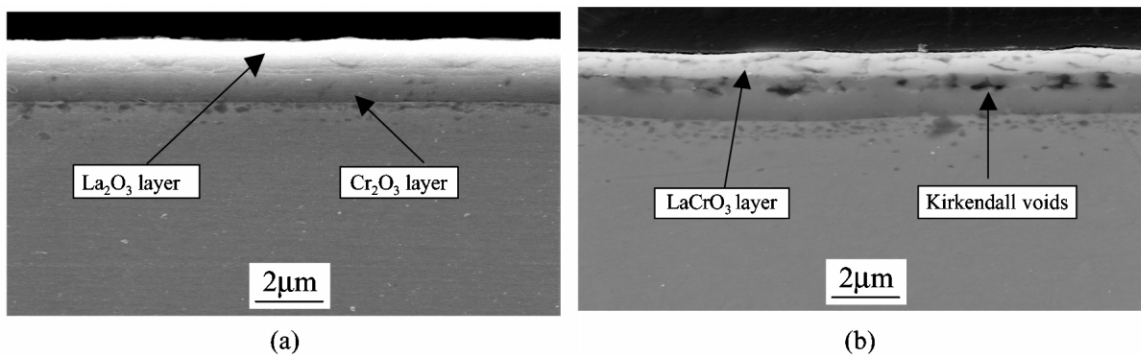


Fig. 2. SEM cross-sectional view of (a) double-layer structure of sputtered  $\text{La}_2\text{O}_3$  layer and thermally grown  $\text{Cr}_2\text{O}_3$  layer and (b)  $\text{LaCrO}_3$  layer formed upon annealing of the double-layer coating.

could be indexed as from  $\text{Cr}_2\text{O}_3$  and some amount of spinel phase formed during the annealing process in low partial pressure oxygen. Furthermore, there were several peaks at  $2\theta = 15.65^\circ$ ,  $27.22^\circ$  and  $27.97^\circ$ , which were indexed as the peaks from the  $\text{La}(\text{OH})_3$  phase. Apparently, this phase was formed during air exposure of the sputtered sample.  $\text{La}_2\text{O}_3$  phase is prone to absorption of moisture when exposed in air, leading to the formation of the  $\text{La}(\text{OH})_3$  phase. After annealing at  $800^\circ\text{C}$  for 10 min (Fig. 3b), these peaks disappeared, due to the desorption of moisture. Interestingly, no peaks could be detected from  $\text{La}_2\text{O}_3$ , possibly due to the amorphous nature or texture of the as-deposited  $\text{La}_2\text{O}_3$  layer. It is quite common to obtain amorphous layer by sputtering due to the rapid cooling rate of the coating on the substrate. After anneal at  $800^\circ\text{C}$  for 1 h in air, strong peaks corresponding to the  $\text{LaCrO}_3$  phase were observed (Fig. 3d). Further increase in annealing time increased

the intensity of these peaks (Fig. 3e), indicating further reaction between the  $\text{La}_2\text{O}_3$  and  $\text{Cr}_2\text{O}_3$  layers. With increase in annealing temperature, the time required for the formation of  $\text{LaCrO}_3$  layer was reduced. Apparently, the reactive formation process is feasible to synthesize the  $\text{LaCrO}_3$  coatings.

### 3.2. Sol-gel processing

Solution-based sol-gel approach for forming the  $\text{LaCrO}_3$ -based coatings is very desirable, as it is a simple process with no costly equipment involved. Therefore, the sol-gel process for synthesizing the doped  $\text{LaCrO}_3$  coatings was systematically investigated. To study the gradual evolution of the coating phase structure during firing and to define the optimal firing conditions, the samples after spin coating with the 0.5 M solution was heated in air in the high-temperature XRD specimen

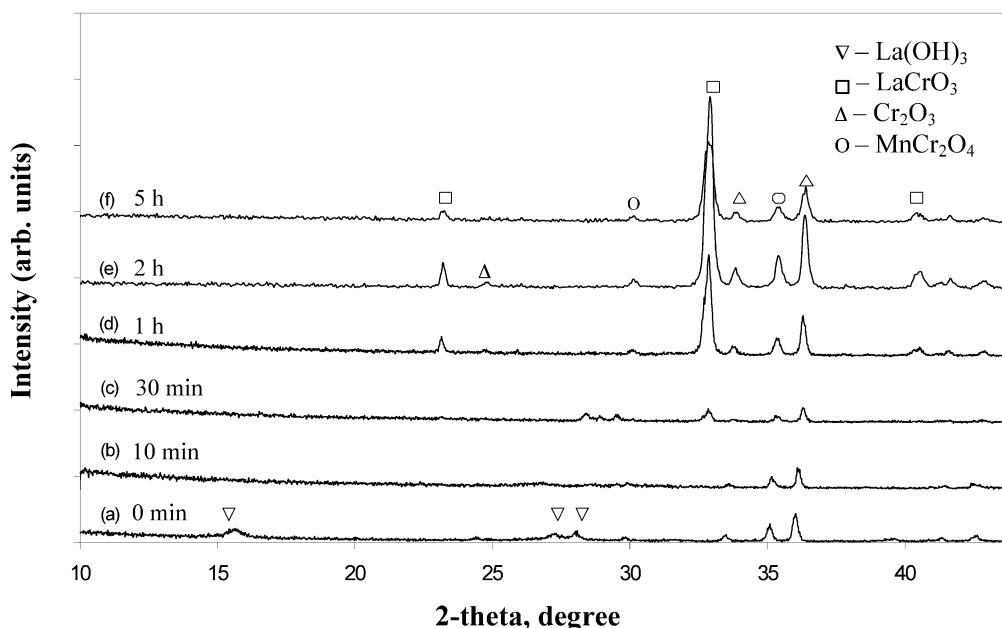


Fig. 3. XRD patterns after annealing in air at  $800^\circ\text{C}$  for different times: (a) as-deposited; (b) 10 min; (c) 30 min; (d) 1 h; (e) 2 h and (f) 5 h.

chamber and XRD patterns were captured in situ during holding of the sample at different temperatures. Fig. 4 shows the high-temperature in-situ XRD results for the sample coated with  $(\text{La}_{0.8}\text{Sr}_{0.2})\text{CrO}_3$ . It can be seen that the reaction started at approximately 600 °C and the perovskite  $(\text{La}_{0.8}\text{Sr}_{0.2})\text{CrO}_3$  phase was formed at 800 °C. Further increase in the temperature to 1000 °C did not change the phase structure significantly; upon cooling to room temperature, the  $(\text{La}_{0.8}\text{Sr}_{0.2})\text{CrO}_3$  phase remained stable. Apparently, firing at 800 °C is sufficient to obtain the  $(\text{La}_{0.8}\text{Sr}_{0.2})\text{CrO}_3$  phase in the coating.

With high solution concentration (e.g. 0.5 M) the coating was thicker, but was more porous; on the other hand, it was found that at low solution concentration (e.g. 0.1 M), the coating thickness per pass was reduced, yet the resulting coating was more dense and uniform. A compromise between the coating thickness and the integrity was reached with a 0.3 M solution. Fig. 5 shows the SEM surface morphologies of the  $\text{LaCrO}_3$  coatings (dip-coated with 0.3 M solution) after six passes with an intermediate anneal of 800 °C for 1 h in air, indicating relatively smooth and uniform coating surface. Subsequently, such coatings were selected for further characterization in Section 3.3.

### 3.3. Electrical resistance and oxidation behavior

The area-specific electrical resistance (ASR) measured using four-point DC method reflects both the conductivity and the thickness of the surface layer (oxide scale and/or coatings). It is generally assumed that the resistivity of the substrate alloy is negligible compared with that of the thermally grown scale or  $\text{LaCrO}_3$ -type coatings on the surface of the alloys. As a result, the measured ASR includes that of the scale/

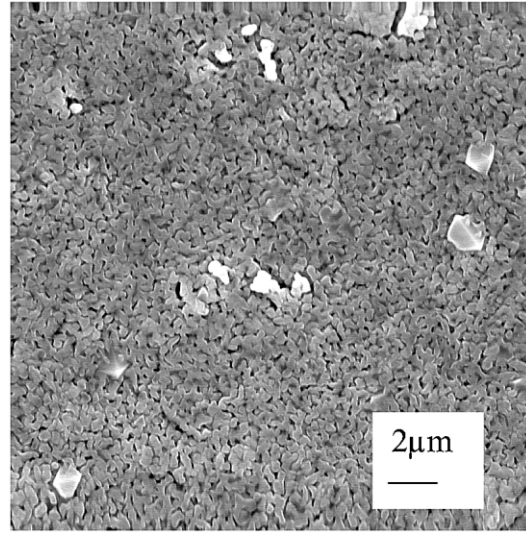


Fig. 5. SEM surface morphologies of the sol-gel coated sample after six passes with intermediate anneal at 800 °C for 1 h.

coating and its interface with the substrate and the Pt electrode. Since the current (0.1 A) is relatively small, interfacial polarization is also negligible. Therefore, the measured ASR is assumed to be that of the scale/coating.

Fig. 6 shows the Arrhenius plot of the  $\text{ASR}/T$  vs. reciprocal of temperature for a number of samples, where 0.0Sr and 0.3Sr denote sol-gel coatings of  $\text{LaCrO}_3$  and  $(\text{La}_{0.7}\text{Sr}_{0.3})\text{CrO}_3$ , respectively. With increase in temperature, the ASR decreased and a linear relationship was found between  $\log(\text{ASR}/T)$  and  $1/T$  for each sample. The results in Fig. 6 indicated that without  $\text{LaCrO}_3$  coating, the oxide scale formed after thermal

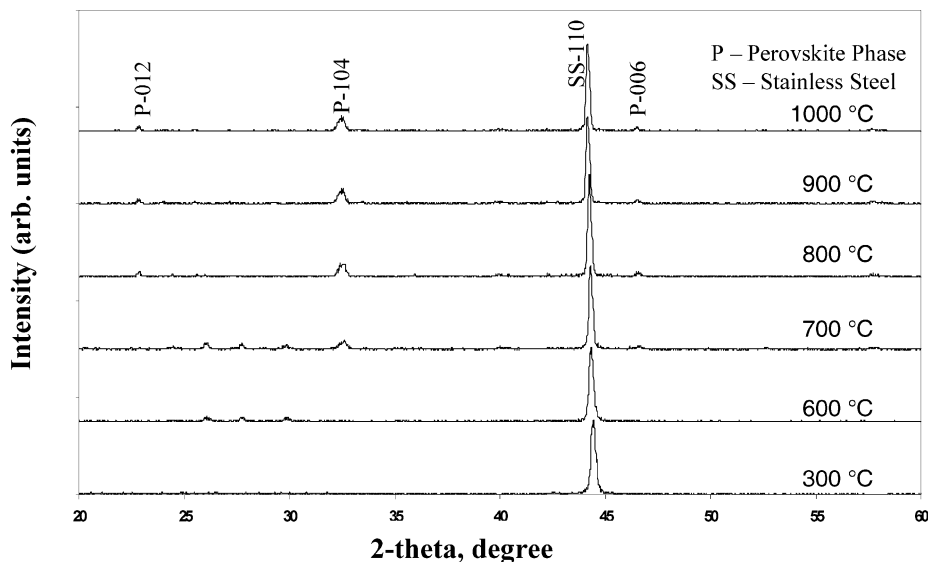


Fig. 4. High-temperature in situ XRD patterns captured during heating of the spin-coated sample.

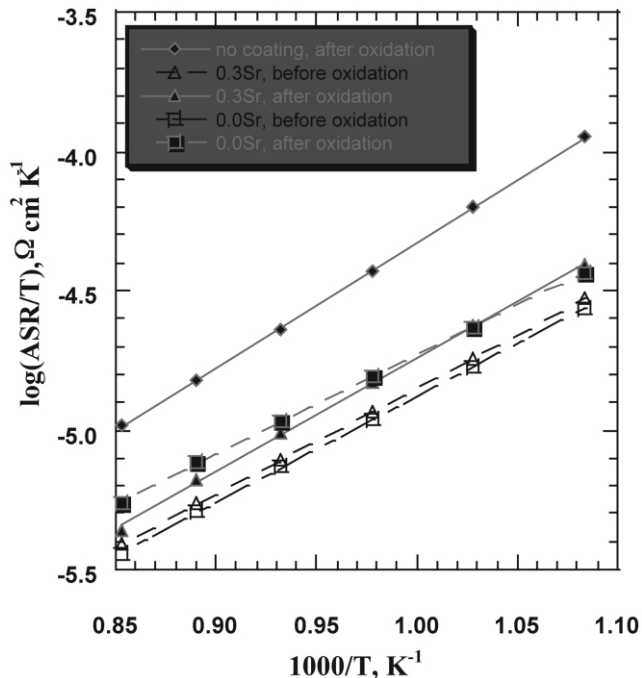


Fig. 6. Arrhenius plot of ASR of coated and/or uncoated samples before and after oxidation in air at 850 °C for 100 h.

exposure at 850 °C for 100 h has a relatively high resistance. With the application of sol-gel ( $\text{La}_{0.7}\text{Sr}_{0.3}\text{CrO}_3$ ) coatings, the electrical resistance of the coating/oxide scale after the same thermal exposure was much lower than that of the bare substrate, clearly indicating the effectiveness of coatings in protecting the substrate from oxidation and in reducing the electrical resistance of the interconnect material. Furthermore, as shown in Fig. 6, the coated samples exhibited small increase in ASR after thermal exposure, which indicated insignificant degradation in electronic conduction during the oxidation and hence the excellent protectiveness of the coatings. Also, from Fig. 6, Sr doping does not affect the electrical conductivity of the  $\text{LaCrO}_3$  coatings, i.e. Sr-doped coatings showed ASR values similar to Sr-free coatings before and after thermal exposure. This is contrary to the common knowledge that Sr doping improves the electrical conductivity of the perovskite phase [24,25]. The fact that the nominal  $\text{LaCrO}_3$  coating is as conductive as the  $(\text{La}_{0.8}\text{Sr}_{0.2})\text{CrO}_3$  coating suggests that we might have a La-deficient  $\text{La}_{1-x}\text{CrO}_3$  phase in the nominal  $\text{LaCrO}_3$  coating. Further study is under way to clarify the effect of Sr on the electrical conductivity of the  $\text{LaCrO}_3$  coating.

The weight changes for coated ( $\text{LaCrO}_3$  and  $(\text{La}_{0.8}\text{Sr}_{0.2})\text{CrO}_3$ ) and bare SS-444 steel samples during cyclic oxidation (twelve 100-h cycles) at 800 °C in air are shown in Fig. 7. Clearly, the coated samples registered consistent weight gain due to oxidation, while the uncoated samples showed weight loss after initial weight

increase. Visual inspection of the oxidized samples indicated that the notable loss of weight for the uncoated samples was due to severe spallation of the oxide scale. Fig. 8 shows the surface morphologies of the oxidized samples with and without coatings. While the bare steel substrate exhibited severe spallation (Fig. 8a), the oxide on the coated samples remained intact after cyclic oxidation (Fig. 8b), presumably due to the reduced oxide scale growth and/or increased scale adhesion.

### 3.4. Comparison of reactive formation and sol-gel process

The reactive formation process has been successfully demonstrated to fabricate the  $\text{LaCrO}_3$  coatings on SS-444 type steel samples. The main advantage of this process is the thermally grown  $\text{Cr}_2\text{O}_3$  layer in low partial pressure of oxygen is thin, dense and highly adherent. It has been shown that the templated growth of  $\text{LaCrO}_3$  via the chemical reaction (Eq. (1)) between the thermally grown  $\text{Cr}_2\text{O}_3$  and physical vapor deposited  $\text{La}_2\text{O}_3$  is feasible and will supposedly inherit the attributes of the  $\text{Cr}_2\text{O}_3$  template. However, there is a drawback of this process. Kirkendall voids could be observed near the initial interface between the  $\text{La}_2\text{O}_3$  and  $\text{Cr}_2\text{O}_3$  layers, which might degrade the integrity of the coating. In addition, introduction of a desired level of Sr dopant in these coatings might be a challenge to using the sputtering technique.

On the other hand, the sol-gel precursor route is a fast and simple process with much less expensive equipments involved. It can be easily scaled up for mass production. Doping with specific levels of elements such as Sr is also straightforward. The feasibility of the sol-gel process for synthesizing the doped  $\text{LaCrO}_3$  coatings has been demonstrated in this work. Initial results

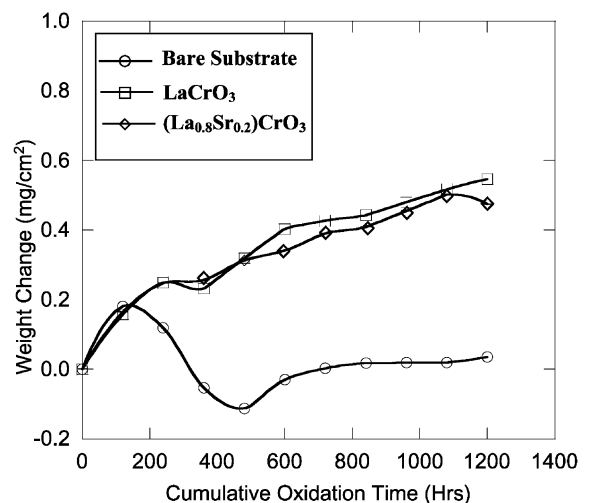


Fig. 7. Weight change vs. cumulative oxidation time during cyclic oxidation (twelve 100-h cycles) at 800 °C in air.

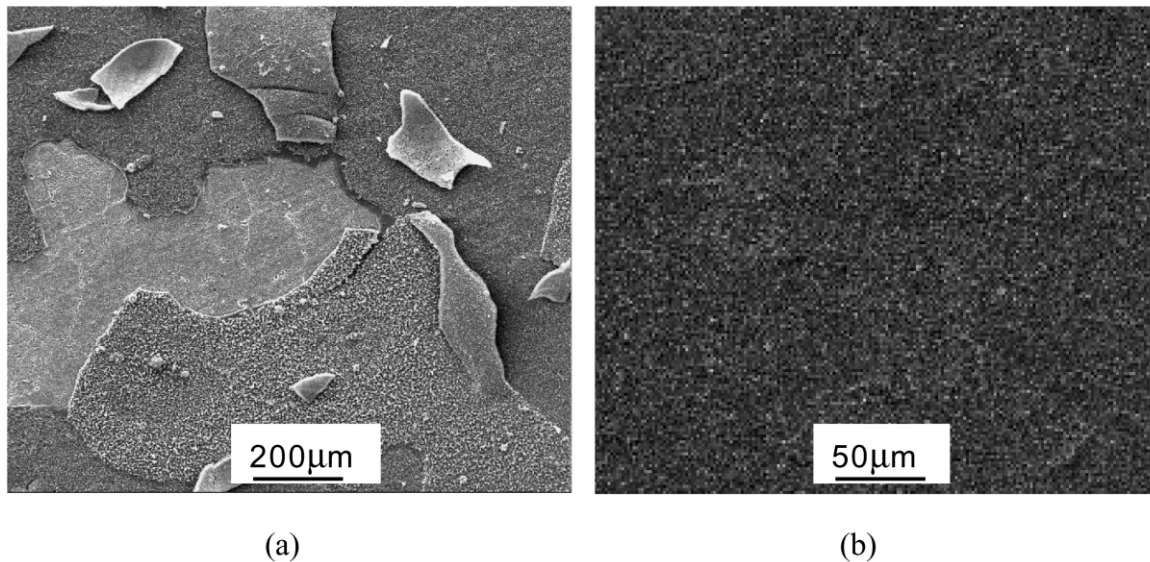


Fig. 8. Surface morphologies of the samples after oxidation of twelve 100-h cycles at 800 °C in air: (a) without coating and (b) with  $(\text{La}_{0.8}\text{Sr}_{0.2})\text{CrO}_3$  coating.

indicated the effectiveness of the sol–gel coatings in reducing the electrical resistance of the oxide formed after thermal exposure and increasing the scale adhesion after cyclic oxidation. Further optimization of the sol–gel process is in progress. Key issues being addressed include (1) finding the best compromise between the coating thickness and the number of passes needed to get the required film thickness; (2) defining the optimal conditions for achieving smooth surface and minimum porosity and (3) more proactive control of the coating stoichiometry and doping level to obtain the coating with best performance.

#### 4. Conclusions

Reactive formation of  $\text{LaCrO}_3$  coating on SS-444 alloy via templated growth from thermally grown  $\text{Cr}_2\text{O}_3$  and sputtered  $\text{La}_2\text{O}_3$  layers has been demonstrated. Several drawbacks of this method have been identified, e.g. the formation of Kirkendall voids in the coating. On the other hand, the sol–gel chelating precursor approach is a simple, cost-effective method for synthesizing the  $\text{LaCrO}_3$ -based coatings on interconnect alloys. The sol–gel coatings improved the oxidation resistance and scale adhesion of the alloy substrate after cyclic oxidation in air at 800 °C, and the coated samples show much lower electrical resistance compared to the uncoated samples after similar thermal exposure for 100 h at 850 °C.

#### Acknowledgments

This research project was financially supported by Honda R&D Americas, Inc. through a Honda Initiation

Grant Award and by National Science Foundation through grant DMR-0238113. Part of this work was also supported by the Center for Manufacturing Research, Tennessee Technological University (TTU) and by the Assistant Secretary for Energy Efficiency and Renewable Energy, Office of FreedomCAR and Vehicle Technologies, as part of the High Temperature Materials Laboratory User Program, Oak Ridge National Laboratory, managed by UT-Battelle, LLC for the US Department of Energy under contract number DE-AC05-00OR22725. Finally, the authors would like to thank R.E. Packingham, TTU, for his assistance in oxidation tests.

#### References

- [1] S.P.S. Badwal, R. Deller, K. Foger, Y. Ramprakash, J.P. Zhang, *Solid State Ionics* 99 (1997) 297.
- [2] S. Linderroth, P.V. Hendriksen, M. Morgensen, N. Langvad, *J. Mat. Sci.* 31 (1996) 5077.
- [3] W.J. Quadackers, H. Greiner, M. Hänsel, A. Pattanaik, A.S. Khanna, W. Malléner, *Solid State Ionics* 91 (1996) 55.
- [4] U.v.d. Crone, M. Hansel, W.J. Quadackers, R. Vaßen, *Fresen. J. Anal. Chem.* 358 (1997) 230.
- [5] K. Huang, J.B. Goodenough, *Solid State Ionics* 129 (2000) 237.
- [6] B.C.H. Steele, *British Cer. Proc.* 56 (1995) 151.
- [7] P.Y. Hou, K. Huang, W.T. Bakker, in: S.C. Singhal, M. Dokiya (Eds.), *Solid Oxide Fuel Cells VI*, ECS, Pennington, NJ, 1999, p. 737.
- [8] S. Linderroth, P.H. Larsen, in: *New Materials for Batteries and Fuel Cells*, MRS Symp. Proc., vol. 575, MRS, Warrendale, PA, USA, 2000, p. 325.
- [9] T. Kadowaki, T. Shiomitsu, E. Matsuda, H. Nakagawa, H. Tsuneizumi, *Solid State Ionics* 67 (1993) 65.

- [10] W.J. Quadackers, T. Malkow, J. Pirón-Abellán, U. Flesch, V. Shemet, L. Singheiser, in: *Proceedings of the Fourth European Solid Oxide Fuel Cell Forum*, A.J. McEvoy, Lucerne, Switzerland, 2000, p. 827.
- [11] M. Ueda, H. Taimatsu, in: *Proceedings of the Fourth European Solid Oxide Fuel Cell Forum*, A.J. McEvoy, Lucerne, Switzerland, 2000, p. 837.
- [12] K. Hilpert, D. Das, M. Miller, D.H. Peck, R. Weiß, *J. Electrochem. Soc.* 143 (1996) 3642.
- [13] S. Linderoth, *High Temp. Mat. Proc.* 17 (1998) 217.
- [14] N. Oishi, Y. Yamazaki, in: *Electrochemical Society Proceedings*, vol. 99–19, 1999, p.759.
- [15] N. Oishi, T. Namikawa, Y. Yamazaki, *Surf. Coat. Technol.* 132 (2000) 58.
- [16] S. Linderoth, *Surf. Coat. Technol.* 80 (1996) 185.
- [17] G. Schiller, R. Henne, R. Ruckdäschel, *J. Nucl. Mat.* 32 (2000) 3.
- [18] K. Huang, P.Y. Hou, J.B. Goodenough, *Mat. Res. Bull.* 36 (2001) 81.
- [19] T. Shiomitsu, T. Kadowaki, T. Ogawa, T. Maruyama, in: M. Dokiya, O. Yamamoto, H. Tagawa, S.C. Singhal (Eds.), *Solid Oxide Fuel Cells IV*, ECS, Pennington, NJ, 1995, p. 850.
- [20] K. Przybylski, J. Prazuch, T. Brzylewski, T. Maruyama, in: *Proceedings of 14th International Corrosion Congress*, 1999, p. 122.
- [21] S.P.S. Badwal, K. Foger, X.G. Zhang, D. Jaffrey, *Fuel Cell Interconnect Device*, US Patent No. 05942349, 1999.
- [22] D. Peck, M. Miller, K. Hilpert, *Solid State Ionics* 143 (2001) 401.
- [23] H. Yokokawa, N. Sakai, T. Kawada, M. Dokiya, *J. Electrochem. Soc.* 138 (1991) 1018.
- [24] M. Mori, T. Yamamoto, H. Itoh, T. Watanbe, *J. Mat. Sci.* 32 (1997) 2423.
- [25] I. Yasuda, *Solid State Ionics* 80 (1995) 141.